Earth's Future

RESEARCH ARTICLE
10.1029/2023EF004246

Special Collection:
CMIP6: Trends, Interactions, Evaluation, and Impacts

Quantifying Global Hydrological Sensitivity to CO_2 Physiological and Radiative Forcings Under Large CO_2 Increases

Xuanze Zhang[1], Yongqiang Zhang[1], Ying-Ping Wang[2], Qiuhong Tang[1], Yunyun Ban[1], Chanyue Ren[1], Husi Letu[3], Jiancheng Shi[4], and Changming Liu[1]

[1]Key Laboratory of Water Cycle and Related Land Surface Processes, Institute of Geographic Sciences and Natural Resources Research, Chinese Academy of Sciences, Beijing, China, [2]CSIRO Environment, Clayton South, VIC, Australia, [3]State Key Laboratory of Remote Sensing Science, Aerospace Information Research Institute, Chinese Academy of Sciences, Beijing, China, [4]National Space Science Center, Chinese Academy of Sciences, Beijing, China

Key Points:

- Global hydrological responses to forcings from rising CO_2-induced physiological and radiative effects were decoupled from CMIP6 models' simulations with 1% per year CO_2 increase
- Global hydrological sensitivity to CO_2 physiological forcing is $-0.09 \pm 0.07\%$ $(100\ ppm)^{-1}$ and to CO_2 radiative forcing is $1.54 \pm 0.24\%\ K^{-1}$ from transient $4 \times CO_2$ simulations
- Global hydrological sensitivities to CO_2 physiological and radiative forcings have little changes over transient $2 \times CO_2$ to $4 \times CO_2$ scenario

Supporting Information:

Supporting Information may be found in the online version of this article.

Correspondence to:

X. Zhang and Y. Zhang,
xuanzezhang@igsnrr.ac.cn;
zhangyq@igsnrr.ac.cn

Citation:

Zhang, X., Zhang, Y., Wang, Y.-P., Tang, Q., Ban, Y., Ren, C., et al. (2024). Quantifying global hydrological sensitivity to CO_2 physiological and radiative forcings under large CO_2 increases. *Earth's Future*, *12*, e2023EF004246. https://doi.org/10.1029/2023EF004246

Received 8 NOV 2023
Accepted 11 NOV 2024

Author Contributions:

Conceptualization: Xuanze Zhang, Yongqiang Zhang, Ying-Ping Wang
Data curation: Xuanze Zhang, Chanyue Ren
Formal analysis: Xuanze Zhang

Abstract Prediction of surface freshwater flux (precipitation or evaporation) in a CO_2-enriched climate is highly uncertain, primarily depending on the hydrological responses to physiological and radiative forcings of CO_2 increase. Using the 1pctCO_2 (a 1% per year CO_2 increase scenario) experiments of 12 CMIP6 models, we first decouple and quantify the magnitude of global hydrological sensitivity to CO_2 physiological and radiative forcings. Results show that the direct global hydrological sensitivity (for land plus ocean precipitation) to CO_2 increase only is $-0.09 \pm 0.07\%$ $(100\ ppm)^{-1}$ and to CO_2-induced warming alone is $1.54 \pm 0.24\%\ K^{-1}$. The latter is about 10% larger than the global apparent hydrological sensitivity (i.e., including all effects, not only direct responses to warming, $\eta_a = 1.39 \pm 0.22\%\ K^{-1}$). These hydrological sensitivities are relatively stable over transient $2\times$ to $4 \times CO_2$ scenario. The intensification of the global water cycle are dominated by the CO_2 radiative effect ($79 \pm 12\%$) with a smaller positive contribution from the interaction between the two effects ($6 \pm 12\%$), but are reduced by the CO_2 physiological effect ($-10 \pm 8\%$). This finding underlines the importance of CO_2 vegetation physiology in global water cycle projections under a CO_2-enriched and warming climate.

Plain Language Summary Projections of future water resource under rising CO_2 and warming scenarios are highly uncertain, which is mainly due to the poor understanding of hydrological responses within the Earth system. We evaluate two major hydrological responses associated with rising CO_2 related effects: physiological effect (e.g., decrease in plant stomatal conductance per unit leaf area, increase in leaf area index and net available energy, etc.) and radiative effect (e.g., rising CO_2-induced warming, rapid atmospheric adjustment and surface energy budget change, etc.). Using 12 Earth system models' experiments, we find that the CO_2 physiological effect will cause ~0.1% decline for precipitation or evaporation per 100 ppm CO_2 increase at a global scale. The CO_2 radiative effect will cause ~1.5% increase for precipitation or evaporation per Kelvin warming. These changing rates of increase or decline are relatively stable with increasing CO_2 forcing. The modeling experiments under high CO_2 forcing project that the intensification of the global water cycle is mainly controlled by the CO_2 radiative effect, but the CO_2 physiological effect and the interaction between the two effects also play important roles.

1. Introduction

The global water cycle is predicted to intensify in the future, owning to rising atmospheric CO_2 concentration and related surface warming driven by anthropogenic greenhouse gases emissions (Allen & Ingram, 2002; Douville et al., 2023; Huntington, 2006; Wentz et al., 2007). This intensification is generally expressed as increases in surface hydrological fluxes (e.g., precipitation, evapotranspiration, and runoff) with an increase in spatial variability of surface water budget (e.g., precipitation minus evapotranspiration) (Allan, 2023; Zaitchik et al., 2023). Although historical long-term response of precipitation and evapotranspiration to global warming is still ambiguous, recent studies provide some evidence to support an intensifying water cycle, for example, increased trends in extreme river flow (Gudmundsson et al., 2021), observed global surface salinity changes (Durack et al., 2012), and observed increases of global oceanic precipitation and evaporation (Brutsaert, 2017; Wang et al., 2021; Wentz et al., 2007). Climate models also project strong increases in surface hydrological fluxes, for example, global lake evaporation (Wang et al., 2018), global ocean evaporation (Wang et al., 2021), global runoff

Funding acquisition: Yongqiang Zhang, Jiancheng Shi
Methodology: Xuanze Zhang
Project administration: Yongqiang Zhang, Husi Letu, Jiancheng Shi
Supervision: Yongqiang Zhang, Husi Letu, Changming Liu
Validation: Xuanze Zhang
Visualization: Xuanze Zhang
Writing – original draft: Xuanze Zhang
Writing – review & editing: Xuanze Zhang, Yongqiang Zhang, Ying-Ping Wang, Qiuhong Tang, Yunyun Ban, Chanyue Ren, Husi Letu, Jiancheng Shi, Changming Liu

(Alkama et al., 2013; Betts et al., 2007; X. J. Zhang et al., 2014), and global precipitation (Shiogama et al., 2022; Wang et al., 2021) under different atmospheric CO_2 increasing scenarios.

Increased atmospheric CO_2 induces infrared radiative forcing on atmosphere-to-surface energy balance (or "an enhanced greenhouse effect") which further warms the land and ocean surfaces (Myhre et al., 1998, 2013) and alters hydrological processes around most of the world (Cisneros et al., 2014). This "enhanced greenhouse effect" by rising CO_2 is termed as rising CO_2-induced radiative effect in this study. It induces hydrological responses across all timescales including rapid responses from atmospheric adjustments and slow responses with rising CO_2-induced warming and transient climate change (Allan et al., 2020; Douville et al., 2023). One of the hydrological responses is an increase in lower-tropospheric water vapor with a rate of ∼7% per Kelvin warming, driven by increased atmospheric saturation vapor pressure (e_s) and enhanced surface evaporation in response to global warming, as predicted by the Clausius-Clapeyron equation and early global climate models (e.g., Boer, 1993; Held & Soden, 2006). The increased atmospheric water vapor consequently drives an increase of global-mean precipitation with a much smaller growth rate of 1%–3% per Kelvin warming (Allen & Ingram, 2002; Wentz et al., 2007). This smaller rate of increase in precipitation is explained by the suppression from rapid atmospheric adjustments in response to CO_2 radiative effect and cooling effects from scattering aerosols that directly alter the atmospheric energy budget and reduce convective mass fluxes (Allan et al., 2020; Andrews & Forster, 2010; Held & Soden, 2006; Li et al., 2013).

Besides the radiative effect, the increased CO_2 also induces vegetation physiological responses including decrease in stomatal conductance per unit leaf area, and increases in leaf area index (LAI), vegetational cover and growing seasons, and enhanced net available energy at the surface through reduced surface albedo etc. (Guerrieri et al., 2019; Piao, Liu, et al., 2019; Piao, Wang, et al., 2019; X. Z. Zhang et al., 2022). The most significant hydrological response is a decrease in plant transpiration and land evapotranspiration determined by reduced plant stomatal conductance, which further induces regional and large-scale atmospheric vapor transport adjustments and slightly alter global precipitation (e.g., Bounoua et al., 1999; Sellers et al., 1996). This response is also predicted to increase continental runoff (Betts et al., 2007).

The radiative and vegetation physiological effects of rising CO_2 on climate have been proposed and quantified using modeling simulations for an atmospheric CO_2 doubling (abrupt $2 \times CO_2$) scenario (Sellers et al., 1996). Over the last two decades, climate models or earth system models with fully coupled carbon cycle were used to quantify the rising CO_2-induced radiative and physiological effects on global warming, global carbon cycle and carbon-climate feedback (e.g., Betts et al., 1997; Friedlingstein et al., 2003, 2006; Woodward et al., 1998; X. Zhang, Wang, et al., 2021; X. Z. Zhang, Wang, & Zhang, 2023).

Responses of surface hydrological processes to the forcing of rising CO_2-induced radiative effect (termed as "CO_2 radiative forcing") or rising CO_2-induced physiological effect (termed as "CO_2 physiological forcing") also have been studied before (Andrews et al., 2010; Betts et al., 2007; Bonfils et al., 2017; Cao et al., 2010; Richardson et al., 2018; Saint-Lu et al., 2020). For instance, Betts et al. (2007) used an ensemble of experiments with a global climate model (HadSM3) to show that physiological effect of a doubling CO_2 on plant transpiration could increase global mean runoff by 6%. Cao et al. (2010) used another coupled climate model (CCSM3 coupled with CLM3.5/CAM3.5) and found that doubled CO_2 physiological forcing will increase global runoff by ∼8.4% and the forcing from combined radiative and physiological effects resulted in ∼7.35% increase in land precipitation and ∼14.9% increase in runoff. Multi-modeling experiments further emphasized the importance of rising CO_2 physiological effect on global land monsoon rainfall and runoff in a CO_2-enriched climate (Cui et al., 2020).

However, in most previous studies, the hydrological sensitivities of surface hydrological fluxes (e.g., precipitation or evaporation) due to the rising CO_2 radiative and physiological forcings have not been well examined in terms of magnitude and pattern using the state-of-the-art Earth system models. Particularly, the potential interactions between the CO_2 radiative forcing and physiological forcing were ignored in previous studies. The relative roles of the CO_2-radiative and physiological forcings and their interaction remain largely unclear on globe, land or ocean. In this study, we develop a hydrological sensitivity analysis framework to quantify the impacts of CO_2 radiative and physiological forcings and their interaction on global water cycle, using fully or partially coupled simulations by 12 CMIP6 models under a 1% per year increasing atmospheric CO_2 (1pctCO_2) for 140 years (Eyring et al., 2016). With the analysis framework, the strength of the hydrological responses to CO_2 radiative forcing (Friedlingstein et al., 2003; Hansen et al., 1984) is termed as the sensitivity of change in hydrological flux variables (ΔX) to increase in surface air temperature (ΔT). The other is the hydrological responses to the forcing

of surface vegetation, energy and climate changes due to rising CO_2-induced physiological effect. The strength of this hydrological response to CO_2 physiological forcing is termed as the sensitivity of change in hydrological flux variables (ΔX) to increase in atmospheric CO_2 concentration (ΔC).

2. Methods

2.1. Analysis Framework of Rising CO_2-Induced Responses of Global Water Cycle in Earth System

Following the previous frameworks developed for quantifying global carbon cycle——climate feedback (Arora et al., 2013; X. Zhang, Wang, et al., 2021), we develop a similar analysis framework of quantifying global water cycle responding to increasing CO_2 levels by linearly combining the hydrological responses to rising CO_2-induced physiological and radiative forcings and the two forcings' interaction. Potential interactions between the two forcings in the fully coupled Earth system are also considered, which could be very significant at some specific regions. For instance, a potential interaction is that rising CO_2-induced plant growth and LAI increase from CO_2 vegetation physiological effect may further enhance plant transpiration under the surface warming from CO_2-induced radiative forcing (X. Z. Zhang, Zhang, et al., 2021; X. Z. Zhang, Wang, & Zhang, 2023). This effect may increase evapotranspiration, reduce runoff, and alter local precipitation, but how much the interaction affecting hydrological responses is still unknown. Hence, in linear analysis framework of a fully coupled Earth system, change in a hydrological flux variable (ΔX) during a time interval (Δt) since a beginning year (e.g., 1850) can be expressed by

$$\Delta X = \mathrm{B}\Delta C + \Gamma\Delta T + \varepsilon, \tag{1}$$

where X is a hydrological flux variable from the surface perspective, which in this study is annual precipitation (P), evapotranspiration on land or evaporation on ocean (E), or surface water availability ($P - E$) on land, ocean, or global scales. C is annual atmospheric CO_2 concentration and T is annual global-averaged surface air temperature. ε is the interaction contribution between CO_2 physiological and radiative forcings. $\mathrm{B} \equiv \frac{\partial X}{\partial C}$ is the sensitivity parameter due to CO_2 physiological effect (in a unit of mm yr^{-1} $(100\ ppm)^{-1}$), and $\Gamma \equiv \frac{\partial X}{\partial T}$ is the sensitivity parameter due to CO_2 radiative effect (in a unit of mm yr^{-1} K^{-1}). Owing to the different units used for B and Γ, the sensitivity to CO_2 physiological effect and the sensitivity to CO_2 radiative effect are not comparable in this study. Therefore, the hydrological sensitivities to CO_2 concentration only for P, E, and $P - E$ are $B_P = \frac{\partial P}{\partial C}$, $B_E = \frac{\partial E}{\partial C}$, $B_{P-E} = \frac{\partial (P-E)}{\partial C}$, respectively. The hydrological sensitivities to warming alone for P, E, and $P - E$ are $\Gamma_P = \frac{\partial P}{\partial T}$, $\Gamma_E = \frac{\partial E}{\partial T}$, $\Gamma_{P-E} = \frac{\partial (P-E)}{\partial T}$, respectively.

2.2. Calculation of Hydrological Sensitivities From Decoupling Simulations of the CMIP6 1pctCO_2 Experiments

The strength and relative contributions of hydrological responses from the CO_2 physiological forcing and radiative forcing could not be directly estimated, as they interact within the Earth's coupling system of climate, water cycle, and carbon cycle. To date, Earth system models are almost the only effective approach to separate different forcings' contribution to the overall global water cycle responses. To quantify the magnitudes of hydrological sensitivity parameters (i.e., B and Γ) from the global water cycle under rising CO_2-induced forcings, the 1pctCO_2 experiments from the CMIP6 project are ideal decoupling modeling experiments, which provide the fully coupled (COU), the biogeochemically coupled (BGC), and the radiatively coupled (RAD) simulations (Jones et al., 2016). The COU simulations of the "1pctCO_2" configuration include all water cycle and carbon cycle–climate feedbacks driven by transient atmospheric CO_2 increased at a rate of 1% $year^{-1}$ over a 140-year period. By the end of the 140-year simulation, atmospheric CO_2 concentration is quadrupled ($4 \times CO_2$) from the pre-industrial level (~285 ppm at 1850). The BGC simulations of the "1pctCO_2-bgc" configuration are also driven by the prescribed 1% $year^{-1}$ CO_2 forcing, but only the biogeochemical cycle is turned on, meaning that only the CO_2 physiological effect on global water cycle is considered. The RAD simulations of the "1pctCO_2-rad" configuration are driven by the prescribed 1% $year^{-1}$ CO_2 forcing with the CO_2 radiative forcing. Following the approaches for estimating global carbon cycle feedback parameters (Arora et al., 2013; Friedlingstein et al., 2006; X. Zhang, Wang, et al., 2021) and the calculation of apparent hydrological sensitivity (η_a) by Fläschner et al. (2016), the hydrological sensitivity parameter for CO_2 physiological forcing can be estimated by

$$B = \frac{\Delta X^{BGC}\Delta T^{COU} - \Delta X^{COU}\Delta T^{BGC}}{\Delta C^{BGC}\left(\Delta T^{COU} - \Delta T^{BGC}\right)} \approx \frac{\Delta X^{BGC}}{\Delta C^{BGC}}, \quad (2)$$

and hydrological sensitivity parameter for CO_2 radiative forcing is estimated by

$$\Gamma = \frac{\Delta X^{RAD}}{\Delta T^{RAD}}, \quad (3)$$

where X is hydrological flux variable (P, E, and $P - E$). To quantify the contribution of interaction between CO_2 physiological and radiative forcings (the ε term in Equation 1), we calculated differences of the COU, BGC, RAD simulations by

$$\Delta X^{INT} = \Delta X^{COU} - \Delta X^{BGC} - \Delta X^{RAD}, \quad (4)$$

where X is temperature or hydrological flux variable (P, E, and $P - E$).

Simulations from 12 CMIP6 models of the 1pctCO_2 experiments are used in this study. These models include all required outputs of the three experiments (1pctCO_2, 1pctCO_2-rad, 1pctCO_2-bgc) and are available for download via https://esgf-node.llnl.gov/search/cmip6/. They are ACCESS-ESM1-5 (Ziehn et al., 2020), BCC-CSM2-MR (Wu et al., 2019), CESM2 (Danabasoglu et al., 2020), CMCC-ESM2 (Cherchi et al., 2018), CNRM-ESM2-1 (Séférian et al., 2019), GISS-E2-1-G (Ito et al., 2020), IPSL-CM6A-LR (Boucher et al., 2020), MIROC-ES2L (Hajima et al., 2020), MPI-ESM1-2-LR (Mauritsen et al., 2019), MRI-ESM2-0 (Yukimoto et al., 2019), NorESM2-LM (Seland et al., 2020), and UKESM1-0-LL (Sellar et al., 2019). We calculate all hydrological sensitivity parameters at transient 4 × CO_2 (i.e., 1% year^{-1} CO_2 increase up to 4 × CO_2) from monthly outputs of the COU, BGC, and RAD simulations of the 12 CMIP6 models, and perform comparative analysis on global, land and ocean scales across models.

3. Results

3.1. Responses of Temperature and Hydrological Fluxes to Rising CO_2-Induced Forcings

Figure 1 shows long-term changes of global mean surface air temperature (T_A) driven by increasing CO_2 concentration at the 1% year^{-1} for 140 years. On a global scale (including land and ocean), T_A is persistently increased to 4.62 ± 0.92 K (on ensemble mean ± standard deviation) at transient 4 × CO_2, as estimated from the fully coupled (COU) simulations of 12 CMIP6 models. The temperature growth curve indicates the non-linear dependence of radiative forcing upon the increasing CO_2 concentration from 1 × CO_2 to 4 × CO_2 (Myhre et al., 1998). Compared to this warming, global land surface warming is higher, with an estimate of 6.51 ± 1.29 K, and the global ocean surface has a smaller warming of 3.93 ± 0.82 K (Figures 1a and 1b). Decoupling experiments show that the CO_2 radiative forcing almost dominates the global warming in fully coupled simulations with ∼96% contributions for globe and land and ∼98% for ocean (Figures 1e and 1f). By comparison, the CO_2 physiological forcing (from the BGC simulations) induces only small warming of about 0.34 ± 0.28 K on land, and 0.12 ± 0.21 K on ocean at 4 × CO_2 (Figures 1c and 1d). This small warming is mainly contributed by decreased latent heat flux as a result of reduced vegetational stomatal conductance in response to CO_2 increase (Ainsworth & Long, 2005; Bounoua et al., 1999; Cao et al., 2010).

Global mean annual P and E (including land and ocean) increase at the same rate of 8.63 ± 2.89 mm year^{-1} per 100 ppm CO_2 or 15.53 ± 2.48 mm year^{-1} per Kelvin warming (see Figure S1 in Supporting Information S1 for the linear approximations), from the fully coupled simulations of CMIP6 models at the transient 4 × CO_2, due to the overall surface water balance on Earth (Figure 2). This result indicates the global apparent hydrological sensitivity (η_a) is 1.39 ± 0.22% per Kelvin warming, which includes all rising CO_2-induced effects, not just the effect of warming alone. However, the global land surface shows an increased $\Delta(P - E)$ along with CO_2 increase due to much higher increases in P compared to E on land, with $P - E$ increased at a rate of 8.14 ± 4.01 mm year^{-1} (100 ppm CO_2)$^{-1}$. Global ocean surface shows a declined $\Delta(P - E)$ along with CO_2 increase at a rate of −3.99 ± 2.00 mm year^{-1} (100 ppm CO_2) $^{-1}$ (Figures 2a, 2d and 2g).

10.1029/2023EF004246

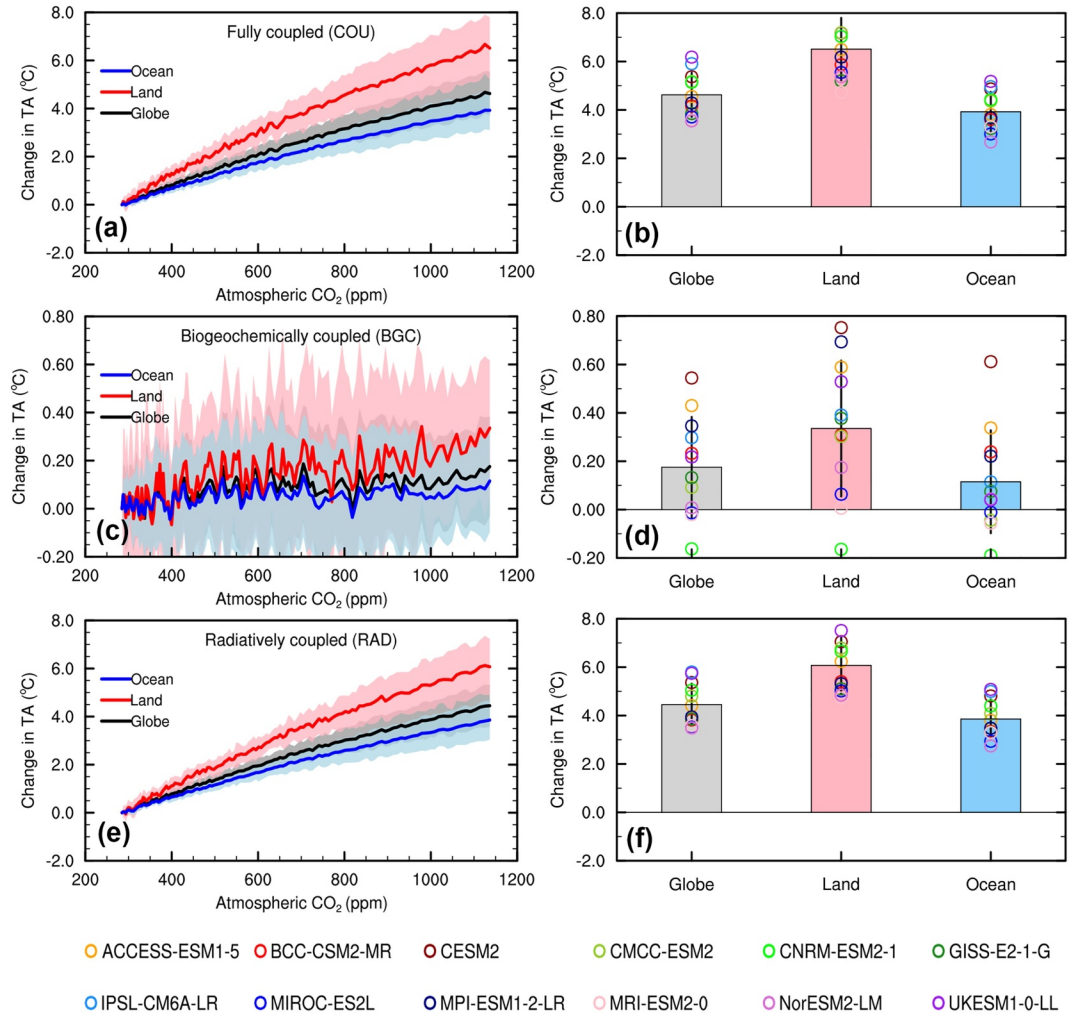

Figure 1. Changes in global annual T_A under transient 1%/year increasing CO_2 forcing scenario. Changes in surface air temperature (ΔT_A) were calculated on global, land and ocean scales, respectively, from (a and b) the fully coupled (COU) simulations, (c and d) the biogeochemically coupled (BGC) simulations, and (e and f) the radiatively coupled (RAD) simulations of the CMIP6 1pctCO_2 experiments. (a, c, e) Time-series of ensemble mean ± standard deviation ΔT_A of 12 CMIP6 models with atmospheric CO_2 increasing from the preindustrial level of 285 ppm to its quadruple ($4 \times CO_2$) over a 140-year period. (b, d, f) CMIP6 modeled ΔT_A at $4 \times CO_2$ for the COU, BGC, RAD simulations, respectively.

Regionally, spatial patterns of the $\Delta(P - E)$ ensemble mean at transient $4 \times CO_2$ (Figure 3) show that the largest wetting land regions are tropical African (10°S–10°N, 5°E–30°E) and Asian rainforests (10°S–10°N, 90°E–140°E), South Asia (10°N–30°N, 70°E–100°E), eastern North America (30°N–45°N, 80°W–90°W) and Western North American area (50°N–70°N, 140°W–160°W). The largest drying land regions are Amazonian rainforests (10°S–10°N, 50°W–80°W), semi-arid regions over continental Europe (30°N–55°N, 0°E–30°E) and southern Africa (10°S–30°S, 10°E–35°E) (Figure 3g). Most regions with negative $\Delta(P - E)$ over oceans are latitude zones of −10°S to −40°S and 10°N to 40°N which covers the conventional oceans with low amount of multi-year mean annual precipitation (Figures 3d and 3g). However, the largest increased $\Delta(P - E)$ over oceans are over the intertropical convergence zone (ITCZ), Southern Ocean (−50°S to −70°S) and northern North Atlantic Ocean (Figure 3g). The strong increased $\Delta(P - E)$ over northern North Atlantic Ocean (40°N–60°N, 20°W–50°W) driven by a large reduction in E (Figures 3d and 3g) is probably due to the North Atlantic warming hole that is linked to a slowdown of the Atlantic meridional overturning circulation (Keil et al., 2020; Rahmstorf et al., 2015).

Decoupling experiments from the RAD and BGC simulations at $4 \times CO_2$ show that most drying/wetting regions are primarily due to the rising CO_2-induced radiative forcing (Figures 3 and 5, and Figure S2 in Supporting

10.1029/2023EF004246

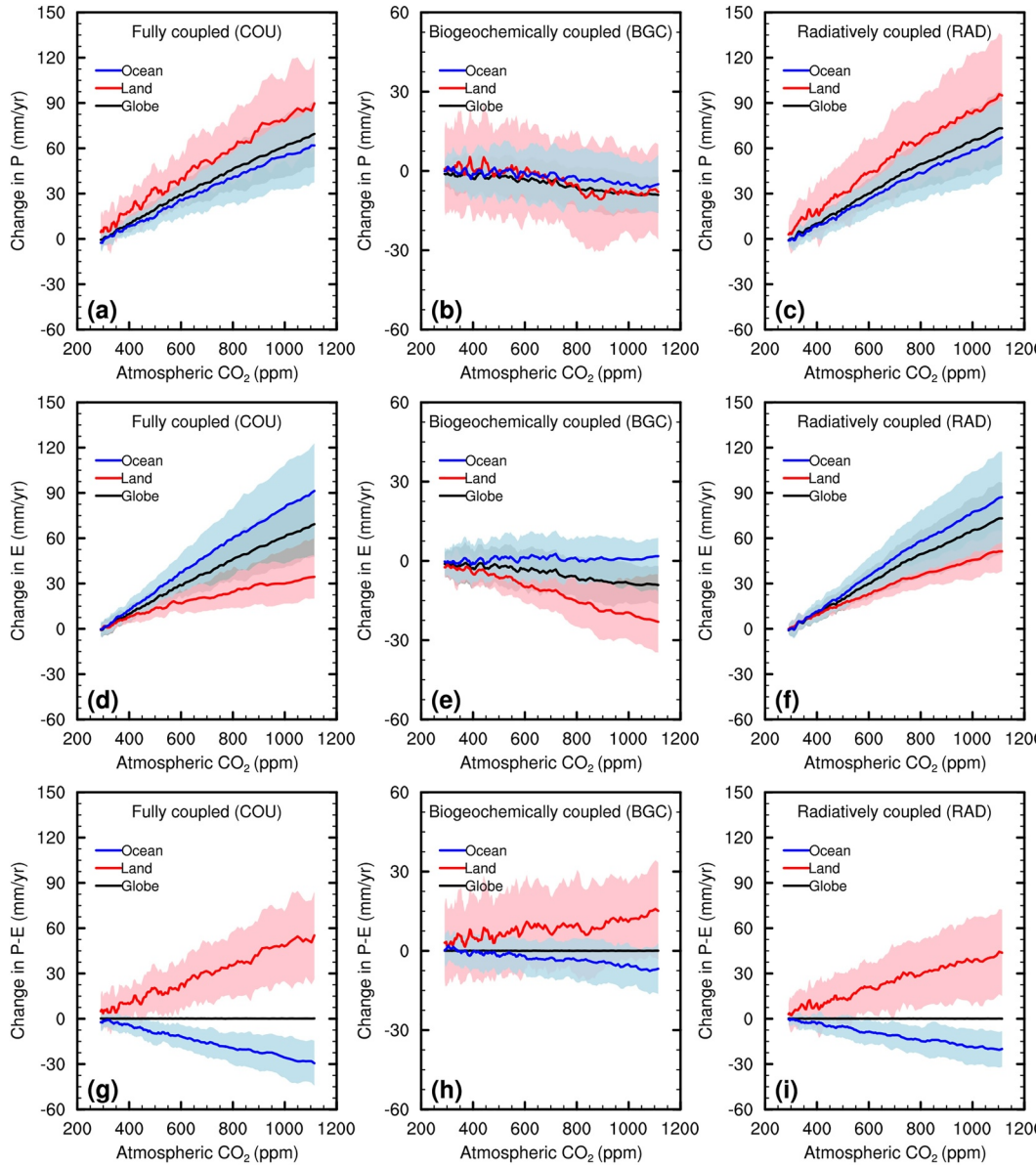

Figure 2. Time series of global annual P, E, and $P - E$ changes under transient 1%/year increasing CO_2 forcing scenario. (a) Changes in precipitation (ΔP) from the COU simulations, and (b) from the BGC simulations due to CO_2 physiological effect, and (c) from the RAD simulations due to CO_2 radiative effect. (d–f) Same as (a–c) but for changes in evaporation (ΔE). (g–i) Same as (a–c) but for differences between precipitation and evaporation ($\Delta(P - E)$). Shaded area represents mean ± standard deviation from 12 CMIP6 models. All series were smoothed with a 5-year moving average.

Information S1) that induces the expansion of Hadley Cells (Grise & Davis, 2020; Schmidt & Grise, 2017) and alters the strength of tropical atmospheric circulations, cloud feedbacks and vapor transport (Collins et al., 2010; Vecchi et al., 2006) which largely shift the meridional distributions of P by increasing P over −10°S–10°N around the equator and by reducing P over latitude zones of 10°S–40°S and 10°N–40°N (Figure 3). Interestingly, the positive $\Delta(P - E)$ of the northern North Atlantic Ocean (Figure 3g) is due to strong reduction of evaporation derived from the CO_2 radiative forcing, although there is smaller decrease in P over the northern North Atlantic Ocean (Figures 3a–3c). Notably, the CO_2 physiological forcing (BGC) consistently causes a decreased land evaporation by reduced plant transpiration from CO_2 stomatal effects as shown in Figure 2e, but causes a drying up of Amazonian rainforests (10°S–10°N, 50°W–80°W) and southern African semi-arid regions (10°S–30°S,

10.1029/2023EF004246

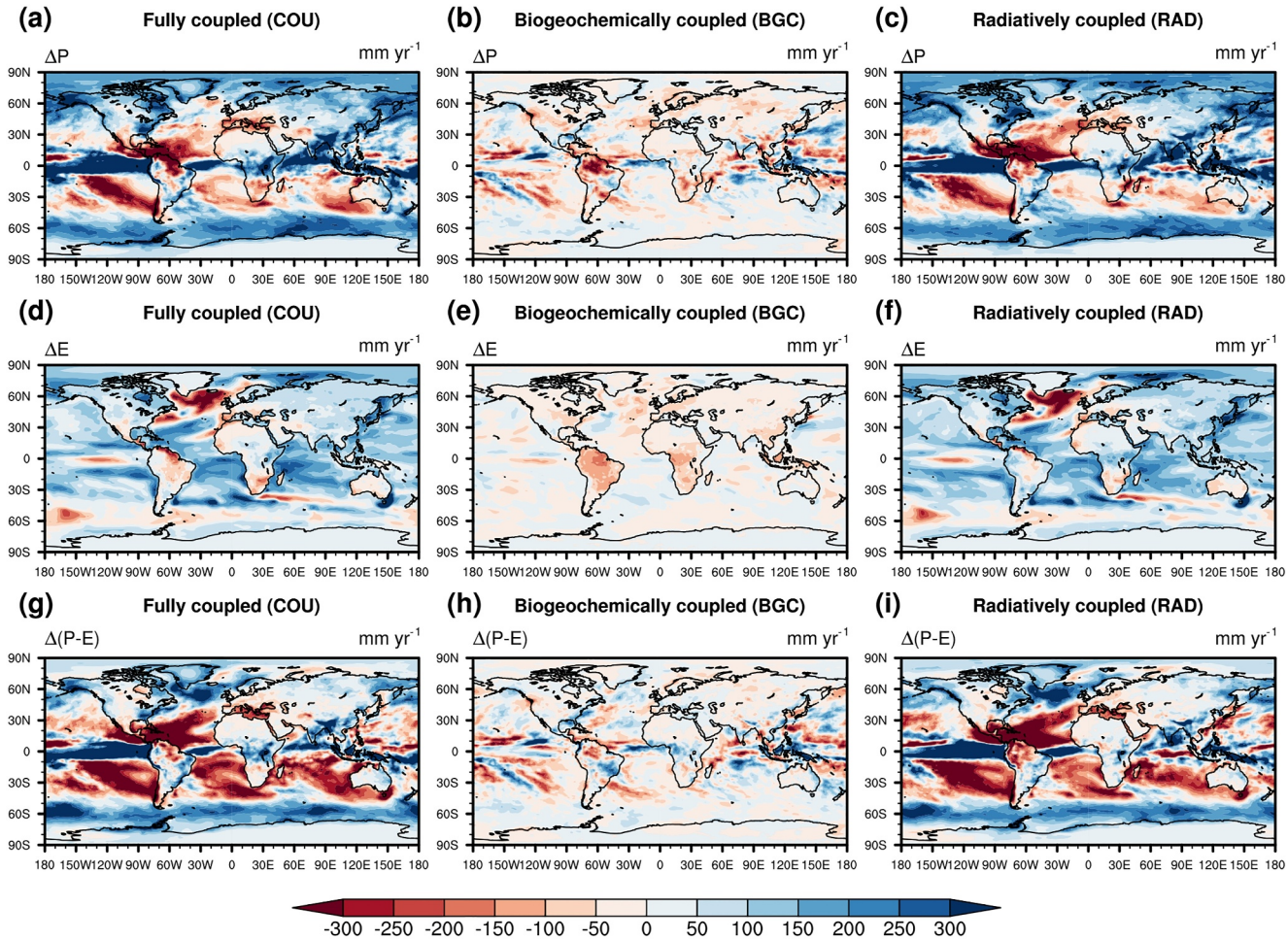

Figure 3. Spatial patterns of long-term changes in P, E, and $P - E$ at transient $4 \times CO_2$. (a) Changes in precipitation (ΔP) from the COU simulations, (b) from the BGC simulations due to CO_2 physiological effect, and (c) from the RAD simulations due to CO_2 radiative effect. (d–f) Same as (a–c) but for changes in evaporation (ΔE). (g–i) Same as (a-c) but for $\Delta(P - E)$. All results are averaged from 12 CMIP6 models of the 1pctCO_2 experiments.

10°E–35°E), which is driven by a larger reduction of precipitation (Figures 3b, 3e, and 3h). Previous study suggested that the reduced precipitation due to CO_2 physiological forcing in Amazonian regions is almost entirely due to repartitioning of sensible and latent heat flues (Richardson et al., 2018).

The interaction between the CO_2 physiological and radiative forcings (Equation 4), as estimated by the ensemble of 12 CMIP6 models, indicates relatively small changes with atmospheric CO_2 forcing increase for P and E on globe, land and ocean (Figures 4a, 4c, and 4e). However, with CO_2 forcing increased to $4 \times CO_2$, the impacts of the interaction have comparable contribution as the CO_2 physiological forcing at regional scales (Figures 4 and 5, and Figure S1 in Supporting Information S1). Regionally, the interactions for P and $P - E$ are strong positive anomalies (200–300 mm yr^{-1}) in Amazonian rainforests and are strong negative anomalies (<−300 mm yr^{-1}) over tropical western Pacific Ocean (5°S–15°N, 120°E–150°E). The northern (southern) areas of the ITCZ over tropical Indian Ocean (20°S–10°N, 60°E–110°E) and tropical Atlantic Ocean (10°S–10°N, 120°E–150°E) show strong positive (negative) anomalies of P and $P - E$ (Figures 4b, 4d and 4f). Overall, the interaction-induced drying or wetting effects (anomaly of $P - E$) over land and oceans are mainly driven by the changes of precipitation. This could be explained by that the regional large changes of precipitation triggered by CO_2 radiative forcing were further disturbed by CO_2 physiological forcing-induced responses in many processes, for example, local to large-scale convective activities, atmospheric precipitable water changes, atmospheric circulation anomalies, etc.

10.1029/2023EF004246

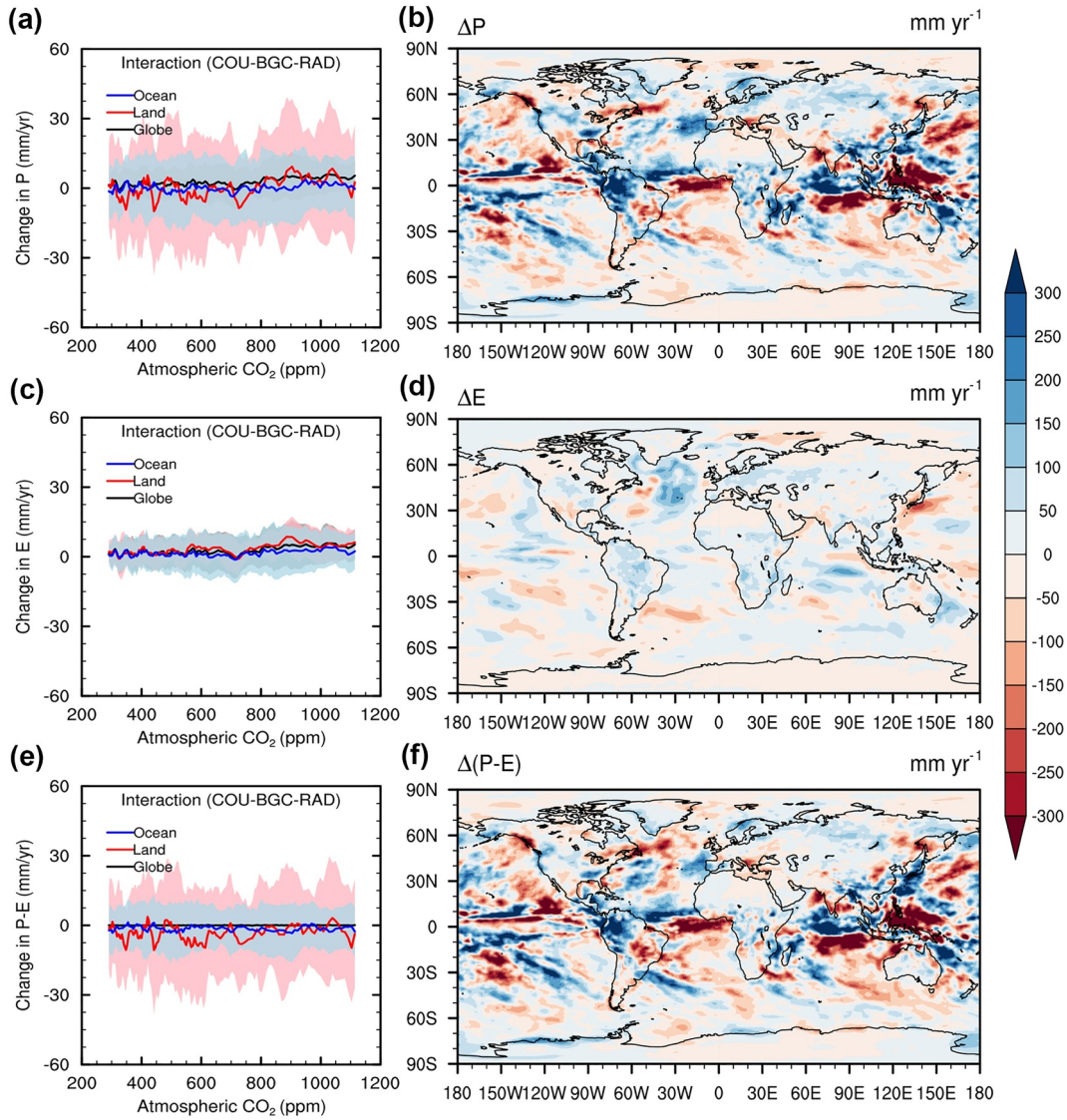

Figure 4. Changes in P, E, and $P - E$ due to interactions between CO_2 physiological and radiative forcings under transient 1%/year increasing CO_2 forcing scenario. (a) Time series of changes in annual precipitation (ΔP) from the COU-BGC-RAD simulations. (b) Spatial pattern of ΔP at transient $4 \times CO_2$. (c and d) Same as (a and b) but for changes in evaporation (ΔE). (e and f) Same as (a and b) but for $\Delta(P - E)$. All results are averaged from 12 CMIP6 models of the 1pctCO_2 experiments.

3.2. Hydrological Sensitivity to Increasing CO_2 Physiological and Radiative Effects

We further estimate the magnitudes of hydrological sensitivity parameters due to the CO_2 physiological forcing and radiative forcing under transient $4 \times CO_2$. Figure 6 and Table 1 show the multi-model ensemble estimates of the two sensitivity parameters for P, E, and P-E on globe, land and ocean. Due to global surface hydrological flux balance, the hydrological sensitivity to CO_2 physiological forcing for P (i.e., B_P) and E (i.e., B_E) on globe are negative with the same estimate of -0.97 ± 0.76 mm year^{-1} (100 ppm)$^{-1}$, and the hydrological sensitivity to the CO_2 radiative forcing for P (Γ_P) and E (Γ_E) on globe are positive with 16.84 ± 2.61 mm year^{-1} K^{-1} (Figure 6). This result indicates that the global hydrological sensitivity to warming is $1.54 \pm 0.24\%$ per Kelvin warming (Table 1). The rising CO_2 radiative forcing intensifies global water cycle, but the CO_2 physiological forcing partly weakens the strength by $-0.09 \pm 0.07\%$ per 100 ppm CO_2 increase. At the global scale, the multi-model ensemble indicates that the CO_2 radiative forcing dominates the overall increases of global P or E at transient $4 \times CO_2$ with a contribution of $79 \pm 12\%$. The CO_2 physiological forcing has a negative contribution of $-10 \pm 8\%$, but the

10.1029/2023EF004246

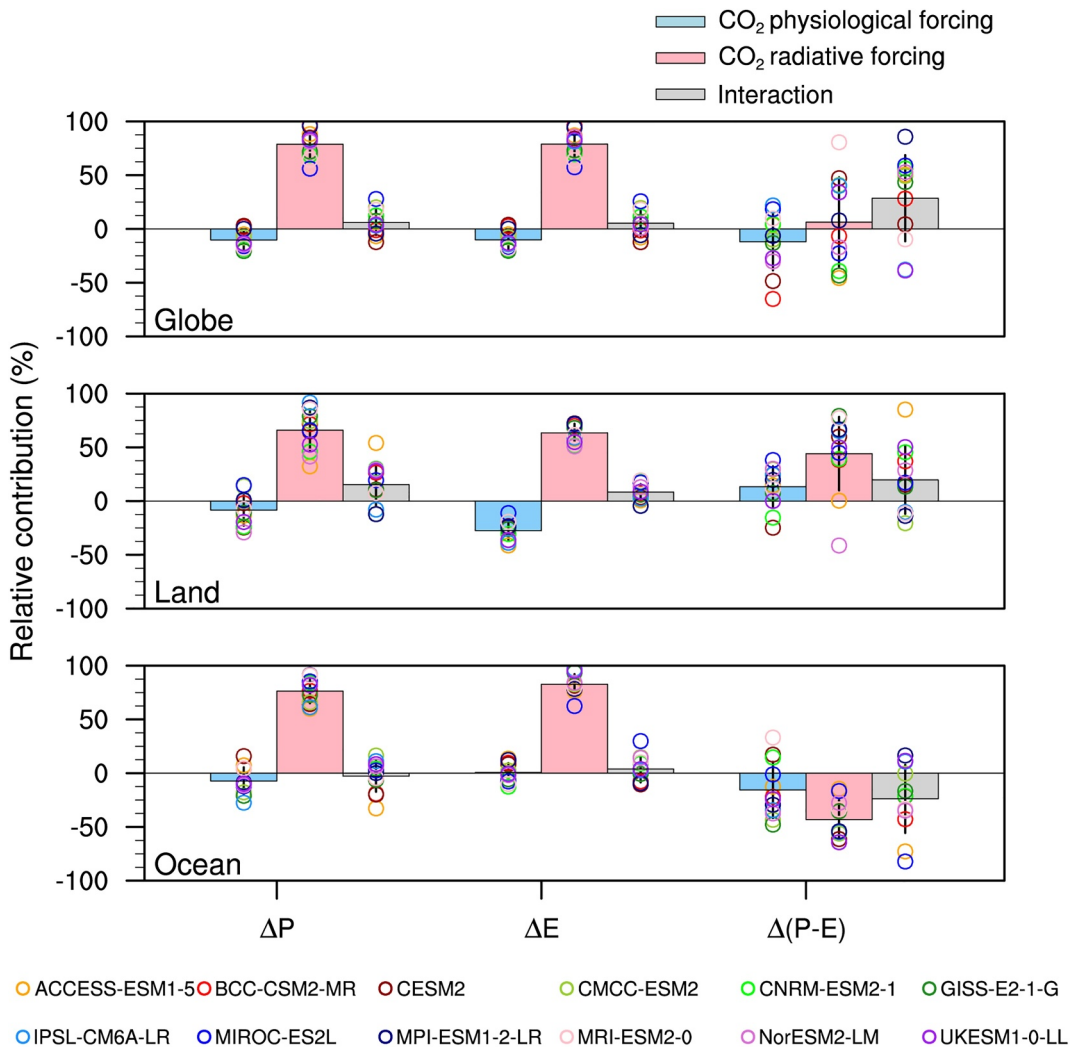

Figure 5. Relative contributions of rising CO_2-induced radiative and physiological forcings to long-term hydrological flux changes at transient 4 × CO_2. Relative contributions to ΔP, ΔE, and $\Delta(P - E)$ are calculated on globe, land and ocean, respectively.

interaction between CO_2 radiative and physiological forcing provides a positive contribution of 6 ± 12% (Figure 5a).

The rising CO_2-induced effects have diverse impacts on water cycles for the land and the ocean surfaces at 4 × CO_2 (Figure 6 and Table 1). On land, the negative response of CO_2 physiological effect for E ($B_{E,L}$) is about 2.5 times larger than the CO_2 physiological effect for P ($B_{P,L}$), which leads to a net positive response of 1.46 ± 1.34 mm $year^{-1}$ (100 ppm) $^{-1}$ for the land water budget ($B_{P-E,L}$) or the CO_2 concentration sensitivity of 0.44 ± 0.39% per 100 ppm CO_2 increase. The CO_2 radiative effect has stronger positive impact on the land water budget for which the sensitivity parameter ($\Gamma_{P-E,L}$) is 6.62 ± 3.53 mm $year^{-1}$ K^{-1} or the temperature sensitivity of 1.90 ± 1.18% per Kelvin warming. The global land surface's wetting (Figures 3g–3i) is dominantly contributed by the CO_2-radiative forcing (44 ± 34%) and enhanced by the CO_2-physiological forcing (13 ± 19%) and their interaction with a significant contribution of 20 ± 32% (Figure 5).

The negative anomalies of water budget (P-E) on global ocean surface (Figures 2g–2i) is primarily driven by the negative response due to the CO_2 radiative forcing that contributes −43 ± 18% of the overall P-E decrease. This negative hydrological response is further enhanced by the CO_2 physiological forcing (−16 ± 26%) and the interaction with a significant contribution of −24 ± 31%. The CO_2-radiative effect on the ocean water budget

10.1029/2023EF004246

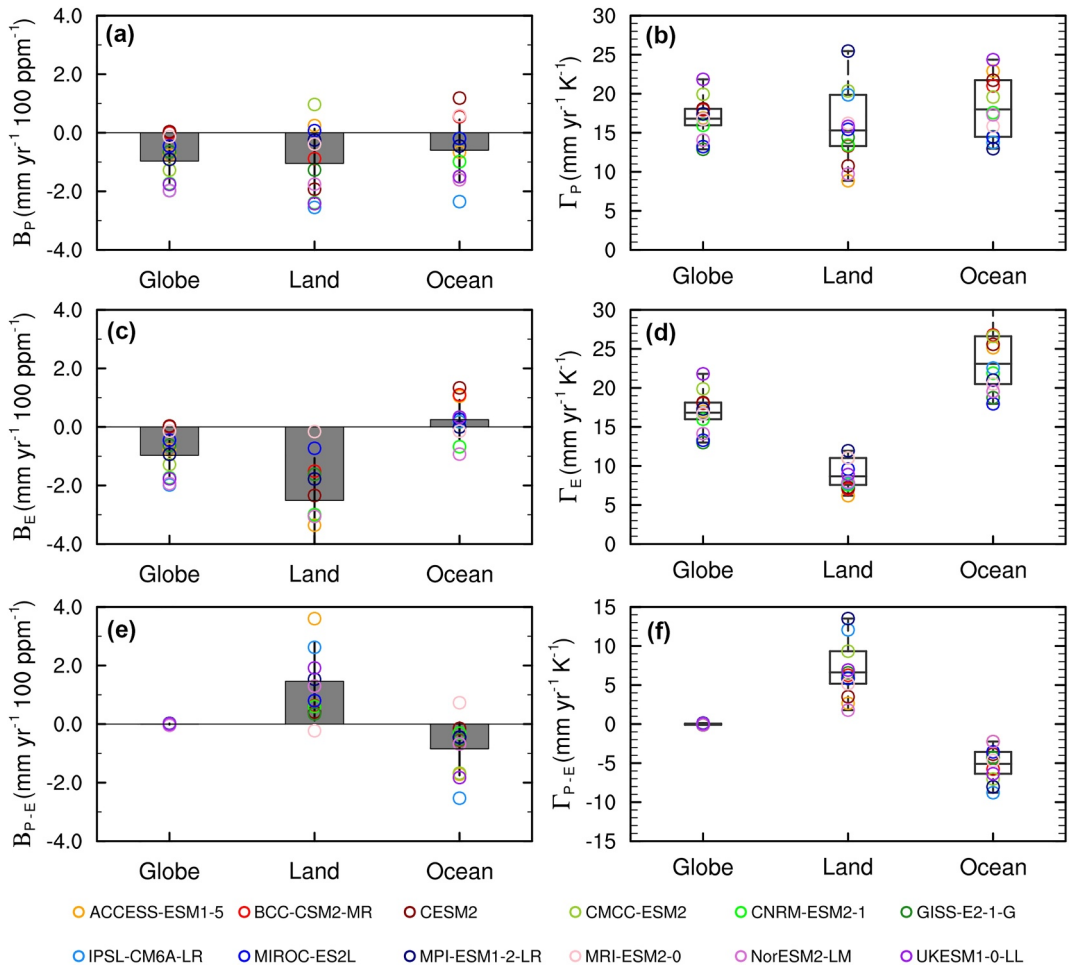

Figure 6. Magnitudes of hydrological sensitivity parameters from rising CO_2-induced radiative and physiological forcings at transient 4 × CO_2. (a) Sensitivity of precipitation to CO_2 physiological forcing (B_P) on globe, land and ocean, respectively. (b) Sensitivity of precipitation to CO_2 radiative forcing (Γ_P) on globe, land and ocean, respectively. (c, e) Same as (a) but for evaporation (B_E) and precipitation minus evaporation (B_{P-E}), respectively. (d, f) Same as (b) but for evaporation (Γ_E) and precipitation minus evaporation (Γ_{P-E}), respectively.

Table 1
Hydrological Sensitivity Parameters From Global Water Cycle Response to Transient 4 × CO_2 Under 1%/Year CO_2 Forcing Scenario

	CO_2 physiological forcing [mm yr^{-1} (100 ppm)$^{-1}$ or (%/100 ppm)]			CO_2 radiative forcing [mm yr^{-1} K^{-1} or (%/K)]		
Parameter[a]	B_P	B_E	B_{P-E}	Γ_P	Γ_E	Γ_{P-E}
Globe	−0.97 ± 0.76	−0.97 ± 0.76	0.00 ± 0.02	16.84 ± 2.61	16.83 ± 2.34	−0.02 ± 0.08
	(−0.09 ± 0.07)	**(−0.09 ± 0.07)**	**(0.00 ± 0.00)**	**(1.54 ± 0.24)**	**(1.54 ± 0.23)**	**(0.00 ± 0.00)**
Land	−1.05 ± 1.18	−2.51 ± 1.45	1.46 ± 1.34	15.30 ± 4.79	8.68 ± 1.83	6.62 ± 3.53
	(−0.13 ± 0.14)	**(−0.53 ± 0.30)**	**(0.44 ± 0.39)**	**(1.91 ± 0.78)**	**(1.81 ± 0.46)**	**(1.90 ± 1.18)**
Ocean	−0.60 ± 1.05	0.25 ± 0.68	−0.84 ± 0.91	17.99 ± 3.86	23.09 ± 3.87	−5.10 ± 2.13
	(−0.05 ± 0.09)	**(0.02 ± 0.05)**	**(0.57 ± 0.57)**	**(1.53 ± 0.31)**	**(1.75 ± 0.28)**	**(3.70 ± 1.61)**

Note. Results are ensemble mean ± s.d. of 12 CMIP6 models. Bold values in () are for percentage changes. [a]Note that B_X is defined as $\frac{\partial X}{\partial C}$, Γ_X is defined as $\frac{\partial X}{\partial T}$, where X are P, E or $P - E$.

($\Gamma_{P-E,O}$) is 3.70 ± 1.61% per Kelvin warming, which is due to the larger positive sensitivity for E ($\Gamma_{E,O}$) than the positive sensitivity for P ($\Gamma_{P,O}$) on oceans (Figure 6, Table 1). However, the negative response by the CO_2-physiological forcing for ocean water budget ($B_{P-E,O}$) is due to the negative sensitivity for P ($B_{P,O}$) and the smaller sensitivity for E ($B_{E,O}$) on ocean (Figure 6).

The above results indicate the global-scale estimates of the two hydrological sensitivities on globe, land and ocean. But how these sensitivities are partitioned to regional scales or latitudinal zones is still unknown. To this end, we further calculated the hydrological sensitivities across latitudinal zones using Equations 2 and 3 from the longitude-averaged ΔP, ΔE, $\Delta(P-E)$, and ΔC, ΔT at transient 4 × CO_2 (Figure S3 in Supporting Information S1). From the zonal average perspective, the global hydrological sensitivity by CO_2-radiative forcing is positively dominated by P and $P-E$ over high latitudes (50°S–70°S) and tropical regions (10°S–10°N) on both land and ocean (Figures S3b and S3f in Supporting Information S1). The hydrological sensitivity by CO_2-physiological forcing is negatively dominated by E over tropical regions (−30°S–15°N) on land, but strongly positively dominated by P and $P-E$ over tropical oceans (10°S–10°N).

3.3. Evolution of Hydrological Sensitivity With Increasing CO_2 Forcing

The above analyses of hydrological sensitivity to CO_2 physiological and radiative effects are based on the long-term changes of hydrological flux variables at transient 4 × CO_2. It is unknown whether the hydrological sensitivities by CO_2 physiological and radiative forcings are consistent over doubling CO_2 forcing levels. To examine whether the global water cycle linearly response to the rising CO_2-induced physiological and radiative forcing, we calculated annual values of global hydrological sensitivity parameters (B and Γ) for P, E, and $P-E$ over the transient 1%/year increasing CO_2 forcing from 1 × CO_2 to 4 × CO_2.

Figure 7 shows that the global hydrological sensitivities by both CO_2 physiological and radiative forcing have little changes over transient 2 × CO_2 (570 ppm) to 4 × CO_2 (1140 ppm) under the 1% per year CO_2 increase scenario. Compared to the parameter values at transient 4 × CO_2 (Figure 6), the global P and E forced by CO_2 physiological effect (B_P and B_E) increase from about −8 mm $year^{-1}$ (100 ppm) $^{-1}$ at 1 × CO_2 (285 ppm) to a relative stable value (about −1 mm $year^{-1}$ (100 ppm) $^{-1}$) at 2 × CO_2, then have little fluctuations over transient 2 × CO_2 to 4 × CO_2 (Figures 7a and 7c). The global hydrological sensitivities to warming or for CO_2 radiative effect feedback (Γ_P and Γ_E) increase to relative stable values early at 1.75 × CO_2 (500 ppm) and have little changes with CO_2 forcing increased to transient 4 × CO_2. The hydrological sensitivities on land and ocean show the similar results. The large changes and uncertainties in global hydrological sensitivity to CO_2 increase or warming over transient 1 × CO_2 to 2 × CO_2 is likely driven by the strong inter-annual variations of global P and E that are modulated by climate internal variability, which covered up the much slower and smaller changes in P and E due to CO_2 increase or warming only. It is also interesting that the global hydrological sensitivity to warming for P (Γ_P) on land and ocean are basically consistent with the global estimate over transient 2 × CO_2 to 4 × CO_2 (Figure 7b). The increased $\Delta(P-E)$ on land or declined $\Delta(P-E)$ on ocean with CO_2 forcing also nearly linearly response to the CO_2 physiological and radiative effects over transient 2 × CO_2 to 4 × CO_2 (Figures 7e and 7f).

4. Discussion and Conclusions

Most previous studies investigated the hydrological sensitivity to global warming in a fully coupled climate system, which is the so called "apparent hydrological sensitivity" (Fläschner et al., 2016), but few separately quantify the temperature sensitivity of hydrological variables solely due to CO_2 radiative effect, and the CO_2 concentration sensitivity of hydrological variables due to CO_2 vegetation physiological effect. For instance, the early versions of climate models predicted that the apparent hydrological sensitivity of global precipitation is in a very likely range of 1%–3% per Kelvin warming (Covey et al., 2003; Douville et al., 2023; Held & Soden, 2006). This model-based range of hydrological sensitivity is still not largely narrowed by recent estimates from CMIP5/6 models (Andrews & Forster, 2010; Douville et al., 2023; Fläschner et al., 2016; Shiogama et al., 2022). In this study, from the fully coupled simulations of 12 CMIP6 models under transient 4 × CO_2, the estimated apparent hydrological sensitivity (η_a) is 1.17%–1.61% per Kelvin warming. It should be noted that the temperature sensitivity of the hydrological transient responses to atmospheric CO_2 increase in this study could be much smaller than those from the stable climate state or the abrupt 4 × CO_2 scenario due to that a transient climate

10.1029/2023EF004246

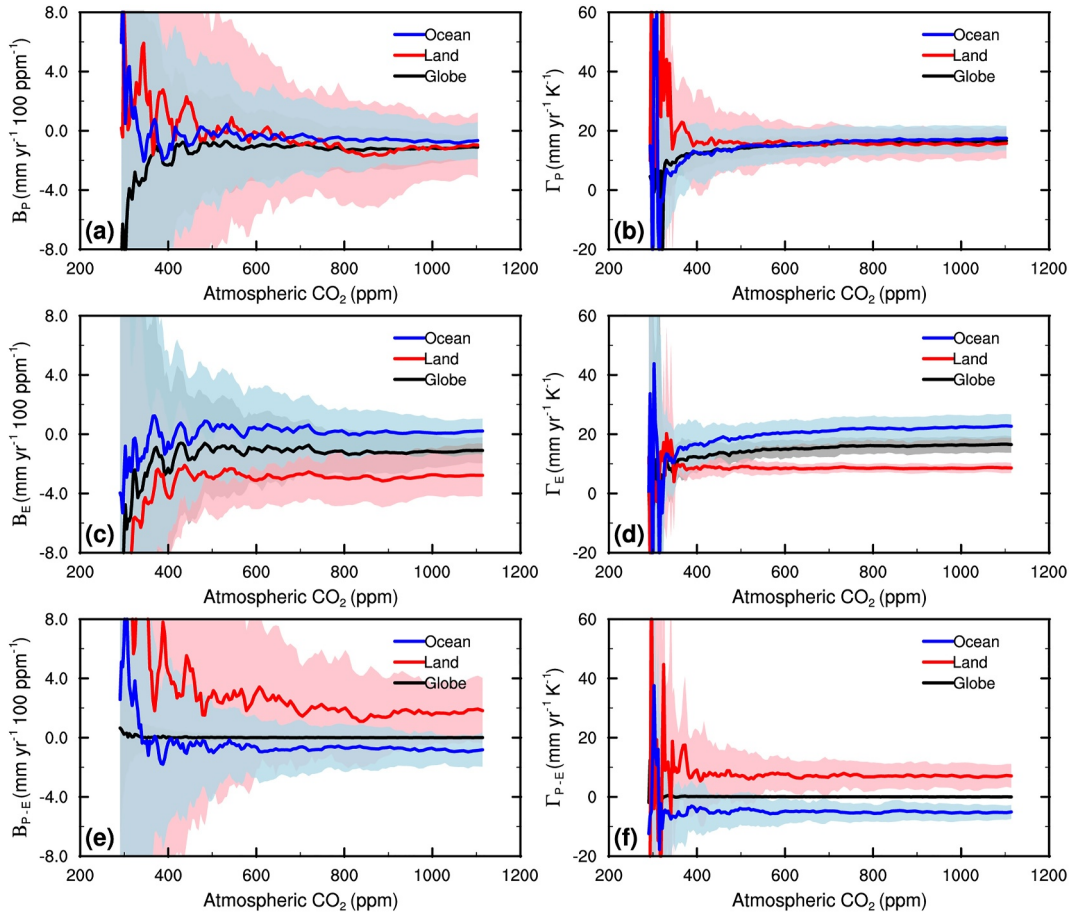

Figure 7. Evolution of hydrological sensitivity parameters from rising CO_2-induced radiative and physiological forcings over transient 1%/year increasing CO_2 forcing ($1 \times CO_2$ to $4 \times CO_2$). (a) Sensitivity of precipitation to CO_2 physiological forcing (B_P) on globe, land and ocean, respectively. (b) Sensitivity of precipitation to CO_2 radiative forcing (Γ_P) on globe, land and ocean, respectively. (c, e) Same as (a) but for evaporation (B_E) and precipitation minus evaporation (B_{P-E}), respectively. (d, f) Same as (b) but for evaporation (Γ_E) and precipitation minus evaporation (Γ_{P-E}), respectively. Shaded area represents mean ± standard deviation from 12 CMIP6 models of the 1pctCO_2 experiments.

induces a fast decreased precipitation response to CO_2 radiative forcing (Andrews & Forster, 2010; Fläschner et al., 2016).

Using the proposed analysis framework of global water cycle in response to rising CO_2, this study defined and quantified the global hydrological sensitivity to rising CO_2-induced physiological and radiative forcings from decoupling simulations of the CMIP6 1pctCO_2 experiments. The CMIP6 models estimated that the global hydrological sensitivity to global warming solely due to the CO_2 radiative forcing is 1.54 ± 0.24% per Kelvin warming, which about 10% larger than the apparent temperature sensitivity calculated from the fully coupled simulations. The global hydrological sensitivity (precipitation or evaporation) by CO_2-physiological forcing is $-0.09 \pm 0.07\%\ (100\ \text{ppm})^{-1}$ at transient $4 \times CO_2$. These global hydrological sensitivities by CO_2 physiological or radiative forcings are relatively stable over transient $2 \times CO_2$ to $4 \times CO_2$, which is consistent with the finding that the apparent hydrological sensitivity to warming has little change at large CO_2 forcing between transient $2 \times CO_2$ and $4 \times CO_2$ (Raiter et al., 2023).

With the CMIP6 1pctCO_2 experiments, this study isolated the relative contributions of rising CO_2-induced physiological and radiative forcings and the interaction between the two to the transient responses of global water cycle to increasing CO_2 forcing. At the global scale, the overall increases of global P or E at transient $4 \times CO_2$ are dominated by the CO_2 radiative forcing (79 ± 12%) and positively contributed by the interaction (6 ± 12%) but are reduced by the CO_2 physiological forcing (−10 ± 8%). On land, the pattern of precipitation minus evaporation

show that the wetting of global land is dominantly contributed by the CO_2 radiative forcing (44 ± 34%) and enhanced by physiological forcing (13 ± 19%) and their interaction (20 ± 32%). In last two decades, a recent study indicated that global water availability (*P-E*) has significantly decreased (Y. Zhang, Li, et al., 2023). The declining trend on land can be reversed for a long period of time, for example, in the transient 4 × CO_2 scenario. However, there are still uncertainties since climate mode changes play a key role in controlling global land water availability. The accuracy of Earth System Models (ESMs) in predicting these climate mode changes is a critical factor for accurately projecting changes in global land water availability. Additionally, 12 model members used in this study may not be the optimal ensemble size to capture robust modeling uncertainty of sensitivity and contribution estimations. Overall, this study quantified hydrological sensitivity to rising CO_2 physiological and radiative forcings and emphasized the importance of CO_2 physiological forcing and interactive effect between physiological and radiative forcings in global water cycle projections under a CO_2-enriched climate.

Data Availability Statement

All simulations of the CMIP6 models for the 1pctCO_2 experiments (Jones et al., 2016) can be freely downloaded from the Earth System Grid Federation (https://esgf-node.llnl.gov/search/cmip6/). The supplementary text, tables, and figures are provided in Supporting Information S1. The additional resulting data set is provided at X. Zhang (2023).

Acknowledgments
This work was supported by the Second Tibetan Plateau Scientific Expedition and Research Program (2019QZKK0206), the National Key Research and Development Program of China (2022YFC3002804), and the Ordos Science & Technology Plan (2022EEDSKJZDZX016). X.Z was supported by the Youth Innovation Promotion Association CAS (2022053) and the Program for the "Kezhen-Bingwei" Youth Talents from IGSNRR CAS (2021RC003).

References

Ainsworth, E. A., & Long, S. P. (2005). What have we learned from 15 years of free-air CO_2 enrichment (FACE)? A meta-analytic review of the responses of photosynthesis, canopy properties and plant production to rising CO_2. *New Phytologist*, *165*(2), 351–371. https://doi.org/10.1111/j.1469-8137.2004.01224.x

Alkama, R., Marchand, L., Ribes, A., & Decharme, B. (2013). Detection of global runoff changes: Results from observations and CMIP5 experiments. *Hydrology and Earth System Sciences*, *17*(7), 2967–2979. https://doi.org/10.5194/hess-17-2967-2013

Allan, R. P. (2023). Amplified seasonal range in precipitation minus evaporation. *Environmental Research Letters*, *18*(9), 094004. https://doi.org/10.1088/1748-9326/acea36

Allan, R. P., Barlow, M., Byrne, M. P., Cherchi, A., Douville, H., Fowler, H. J., et al. (2020). Advances in understanding large-scale responses of the water cycle to climate change. *Annals of the New York Academy of Sciences*, *1472*(1), 49–75. https://doi.org/10.1111/nyas.14337

Allen, M. R., & Ingram, W. J. (2002). Constraints on future changes in climate and the hydrologic cycle. *Nature*, *419*(6903), 224–232. https://doi.org/10.1038/nature01092

Andrews, T., Doutriaux-Boucher, M., Boucher, O., & Forster, P. M. (2010). A regional and global analysis of carbon dioxide physiological forcing and its impact on climate. *Climate Dynamics*, *36*(3–4), 783–792. https://doi.org/10.1007/s00382-010-0742-1

Andrews, T., & Forster, P. M. (2010). The transient response of global-mean precipitation to increasing carbon dioxide levels. *Environmental Research Letters*, *5*(2), 025212. https://doi.org/10.1088/1748-9326/5/2/025212

Arora, V. K., Boer, G. J., Friedlingstein, P., Eby, M., Jones, C. D., Christian, J. R., et al. (2013). Carbon–concentration and carbon–climate feedbacks in CMIP5 Earth system models. *Journal of Climate*, *26*(15), 5289–5314. https://doi.org/10.1175/jcli-d-12-00494.1

Betts, R. A., Boucher, O., Collins, M., Cox, P. M., Falloon, P. D., Gedney, N., et al. (2007). Projected increase in continental runoff due to plant responses to increasing carbon dioxide. *Nature*, *448*(7157), 1037–1041. https://doi.org/10.1038/nature06045

Betts, R. A., Cox, P. M., Lee, S. E., & Woodward, F. I. (1997). Contrasting physiological and structural vegetation feedbacks in climate change simulations. *Nature*, *387*(6635), 796–799. https://doi.org/10.1038/42924

Boer, G. J. (1993). Climate change and the regulation of the surface moisture and energy budgets. *Climate Dynamics*, *8*(5), 225–239. https://doi.org/10.1007/bf00198617

Bonfils, C., Anderson, G., Santer, B. D., Phillips, T. J., Taylor, K. E., Cuntz, M., et al. (2017). Competing influences of anthropogenic warming, ENSO, and plant physiology on future terrestrial aridity. *Journal of Climate*, *30*(17), 6883–6904. https://doi.org/10.1175/JCLI-D-17-0005.1

Boucher, O., Servonnat, J., Albright, A. L., Aumont, O., Balkanski, Y., Bastrikov, V., et al. (2020). Presentation and evaluation of the IPSL-CM6A-LR climate model. *Journal of Advances in Modeling Earth Systems*, *12*(7). https://doi.org/10.1029/2019ms002010

Bounoua, L., Collatz, G. J., Sellers, P. J., Randall, D. A., Dazlich, D. A., Los, S. O., et al. (1999). Interactions between vegetation and climate: Radiative and physiological effects of doubled atmospheric CO_2. *Journal of Climate*, *12*(2), 309–324. https://doi.org/10.1175/1520-0442(1999)012<0309:ibvacr>2.0.co;2

Brutsaert, W. (2017). Global land surface evaporation trend during the past half century: Corroboration by Clausius-Clapeyron scaling. *Advances in Water Resources*, *106*, 3–5. https://doi.org/10.1016/j.advwatres.2016.08.014

Cao, L., Bala, G., Caldeira, K., Nemani, R., & Ban-Weiss, G. (2010). Importance of carbon dioxide physiological forcing to future climate change. *Proceedings of the National Academy of Sciences of the United States of America*, *107*(21), 9513–9518. https://doi.org/10.1073/pnas.0913000107

Cherchi, A., Fogli, P. G., Lovato, T., Peano, D., Iovino, D., Gualdi, S., et al. (2018). Global mean climate and main patterns of variability in the CMCC-CM2 coupled model. *Journal of Advances in Modeling Earth Systems*, *11*(1), 185–209. https://doi.org/10.1029/2018ms001369

Cisneros, J. B. E., Oki, T., Arnell, N. W., Benito, G., Cogley, J. G., Döll, P., et al. (2014). Freshwater resources, in climate change 2014: Impacts, adaptation, and vulnerability. Part A: Global and sectoral aspects. In C. B. Field, V. R. Barros, D. J. Dokken, K. J. Mach, M. D. Mastrandrea, T. E. Bilir, et al. (Eds.), *Contribution of Working Group II to the Fifth Assessment Report of the Intergovernmental Panel on climate change* (pp. 229–269). Cambridge University Press.

Collins, M., An, S.-I., Cai, W., Ganachaud, A., Guilyardi, E., Jin, F.-F., et al. (2010). The impact of global warming on the tropical Pacific Ocean and El Niño. *Nature Geoscience*, *3*(6), 391–397. https://doi.org/10.1038/ngeo868

Covey, C., AchutaRao, K. M., Cubasch, U., Jones, P., Lambert, S. J., Mann, M. E., et al. (2003). An overview of results from the coupled model intercomparison project. *Global and Planetary Change*, *37*(1–2), 103–133. https://doi.org/10.1016/s0921-8181(02)00193-5

Cui, J., Piao, S., Huntingford, C., Wang, X., Lian, X., Chevuturi, A., et al. (2020). Vegetation forcing modulates global land monsoon and water resources in a CO_2-enriched climate. *Nature Communications*, *11*(1), 5184. https://doi.org/10.1038/s41467-020-18992-7

Danabasoglu, G., Lamarque, J. F., Bacmeister, J., Bailey, D. A., DuVivier, A. K., Edwards, J., et al. (2020). The community Earth system model version 2 (CESM2). *Journal of Advances in Modeling Earth Systems*, *12*(2). https://doi.org/10.1029/2019MS001916

Douville, H., Raghavan, K., Renwick, J., Allan, R. P., Arias, P. A., Barlow, M., et al. (2023). Water cycle changes. In V. Masson-Delmotte, P. Zhai, A. Pirani, S. L. Connors, C. Péan, S. Berger, et al. (Eds.), *Climate Change 2021—The physical science basis* (pp. 1055–1210). Cambridge University Press. https://doi.org/10.1017/9781009157896.010

Durack, P. J., Wijffels, S. E., & Matear, R. J. (2012). Ocean salinities reveal strong global water cycle intensification during 1950 to 2000. *Science*, *336*(6080), 455–458. https://doi.org/10.1126/science.1212222

Eyring, V., Bony, S., Meehl, G. A., Senior, C. A., Stevens, B., Stouffer, R. J., & Taylor, K. E. (2016). Overview of the coupled model intercomparison project phase 6 (CMIP6) experimental design and organization. *Geoscientific Model Development*, *9*(5), 1937–1958. https://doi.org/10.5194/gmd-9-1937-2016

Fläschner, D., Mauritsen, T., & Stevens, B. (2016). Understanding the intermodel spread in global-mean hydrological sensitivity. *Journal of Climate*, *29*(2), 801–817. https://doi.org/10.1175/Jcli-D-15-0351.1

Friedlingstein, P., Cox, P., Betts, R., Bopp, L., von Bloh, W., Brovkin, V., et al. (2006). Climate–carbon cycle feedback analysis: Results from the C4MIP model intercomparison. *Journal of Climate*, *19*(14), 3337–3353. https://doi.org/10.1175/jcli3800.1

Friedlingstein, P., Dufresne, J. L., Cox, P. M., & Rayner, P. (2003). How positive is the feedback between climate change and the carbon cycle? *Tellus B: Chemical and Physical Meteorology*, *55*(2), 692–700. https://doi.org/10.1034/j.1600-0889.2003.01461.x

Grise, K. M., & Davis, S. M. (2020). Hadley cell expansion in CMIP6 models. *Atmospheric Chemistry and Physics*, *20*(9), 5249–5268. https://doi.org/10.5194/acp-20-5249-2020

Gudmundsson, L., Boulange, J., Do, H. X., Gosling, S. N., Grillakis, M. G., Koutroulis, A. G., et al. (2021). Globally observed trends in mean and extreme river flow attributed to climate change. *Science*, *371*(6534), 1159–1162. https://doi.org/10.1126/science.aba3996

Guerrieri, R., Belmecheri, S., Ollinger, S. V., Asbjornsen, H., Jennings, K., Xiao, J., et al. (2019). Disentangling the role of photosynthesis and stomatal conductance on rising forest water-use efficiency. *Proceedings of the National Academy of Sciences of the United States of America*, *116*(34), 16909–16914. https://doi.org/10.1073/pnas.1905912116

Hajima, T., Watanabe, M., Yamamoto, A., Tatebe, H., Noguchi, M. A., Abe, M., et al. (2020). Development of the MIROC-ES2L Earth system model and the evaluation of biogeochemical processes and feedbacks. *Geoscientific Model Development*, *13*(5), 2197–2244. https://doi.org/10.5194/gmd-13-2197-2020

Hansen, J., Lacis, A., Rind, D., Russell, G., Stone, P., Fung, I., et al. (1984). Climate sensitivity: Analysis of feedback mechanisms. *Climate Processes and Climate Sensitivity*, *5*, 130–163. https://doi.org/10.1029/GM029p0130

Held, I. M., & Soden, B. J. (2006). Robust responses of the hydrological cycle to global warming. *Journal of Climate*, *19*(21), 5686–5699. https://doi.org/10.1175/JCLI3990.1

Huntington, T. G. (2006). Evidence for intensification of the global water cycle: Review and synthesis. *Journal of Hydrology*, *319*(1–4), 83–95. https://doi.org/10.1016/j.jhydrol.2005.07.003

Ito, G., Romanou, A., Kiang, N. Y., Faluvegi, G., Aleinov, I., Ruedy, R., et al. (2020). Global carbon cycle and climate feedbacks in the NASA GISS ModelE2.1. *Journal of Advances in Modeling Earth Systems*, *12*(10). https://doi.org/10.1029/2019MS002030

Jones, C. D., Arora, V., Friedlingstein, P., Bopp, L., Brovkin, V., Dunne, J., et al. (2016). C4MIP—The coupled climate–carbon cycle model intercomparison project: Experimental protocol for CMIP6. *Geoscientific Model Development*, *9*(8), 2853–2880. https://doi.org/10.5194/gmd-9-2853-2016

Keil, P., Mauritsen, T., Jungclaus, J., Hedemann, C., Olonscheck, D., & Ghosh, R. (2020). Multiple drivers of the North Atlantic warming hole. *Nature Climate Change*, *10*(7), 667–671. https://doi.org/10.1038/s41558-020-0819-8

Li, G., Harrison, S. P., Bartlein, P. J., Izumi, K., & Colin Prentice, I. (2013). Precipitation scaling with temperature in warm and cold climates: An analysis of CMIP5 simulations. *Geophysical Research Letters*, *40*(15), 4018–4024. https://doi.org/10.1002/grl.50730

Mauritsen, T., Bader, J., Becker, T., Behrens, J., Bittner, M., Brokopf, R., et al. (2019). Developments in the MPI-M Earth system model version 1.2 (MPI-ESM1.2) and its response to increasing CO_2. *Journal of Advances in Modeling Earth Systems*, *11*(4), 998–1038. https://doi.org/10.1029/2018MS001400

Myhre, G., Highwood, E. J., Shine, K. P., & Stordal, F. (1998). New estimates of radiative forcing due to well mixed greenhouse gases. *Geophysical Research Letters*, *25*(14), 2715–2718. https://doi.org/10.1029/98gl01908

Myhre, G., Shindell, D., Bréon, F.-M., Collins, W., Fuglestvedt, J., Huang, J., et al. (2013). Anthropogenic and natural radiative forcing. In T. F. Stocker, D. Qin, G.-K. Plattner, M. Tignor, S. K. Allen, J. Boschung, et al. (Eds.), *Climate Change 2013: The Physical Science Basis. Contribution of Working Group I to the Fifth Assessment Report of the Intergovernmental Panel on Climate Change* (pp. 659–740). Cambridge University Press. https://doi.org/10.1017/CBO9781107415324.018

Piao, S., Liu, Q., Chen, A., Janssens, I. A., Fu, Y., Dai, J., et al. (2019). Plant phenology and global climate change: Current progresses and challenges. *Global Change Biology*, *25*(6), 1922–1940. https://doi.org/10.1111/gcb.14619

Piao, S., Wang, X., Park, T., Chen, C., Lian, X., He, Y., et al. (2019). Characteristics, drivers and feedbacks of global greening. *Nature Reviews Earth & Environment*, *1*(1), 14–27. https://doi.org/10.1038/s43017-019-0001-x

Rahmstorf, S., Box, J. E., Feulner, G., Mann, M. E., Robinson, A., Rutherford, S., & Schaffernicht, E. J. (2015). Exceptional twentieth-century slowdown in Atlantic Ocean overturning circulation. *Nature Climate Change*, *5*(5), 475–480. https://doi.org/10.1038/nclimate2554

Raiter, D., Polvani, L. M., Mitevski, I., Pendergrass, A. G., & Orbe, C. (2023). Little change in apparent hydrological sensitivity at large CO_2 forcing. *Geophysical Research Letters*, *50*(18). https://doi.org/10.1029/2023GL104954

Richardson, T. B., Forster, P. M., Andrews, T., Boucher, O., Faluvegi, G., Flaschner, D., et al. (2018). Carbon dioxide physiological forcing dominates projected Eastern Amazonian drying. *Geophysical Research Letters*, *45*(6), 2815–2825. https://doi.org/10.1002/2017gl076520

Saint-Lu, M., Chadwick, R., Lambert, F. H., Collins, M., Boutle, I., Whitall, M., & Daleu, C. (2020). Influences of local and remote conditions on tropical precipitation and its response to climate change. *Journal of Climate*, *33*(10), 4045–4063. https://doi.org/10.1175/jcli-d-19-0450.1

Schmidt, D. F., & Grise, K. M. (2017). The response of local precipitation and sea level pressure to Hadley cell expansion. *Geophysical Research Letters*, *44*(20), 10573–510582. https://doi.org/10.1002/2017GL075380

Séférian, R., Nabat, P., Michou, M., Saint-Martin, D., Voldoire, A., Colin, J., et al. (2019). Evaluation of CNRM Earth system model, CNRM-ESM2-1: Role of Earth system processes in present-day and future climate. *Journal of Advances in Modeling Earth Systems*, *11*(12), 4182–4227. https://doi.org/10.1029/2019MS001791

Seland, Ø., Bentsen, M., Olivié, D., Toniazzo, T., Gjermundsen, A., Graff, L. S., et al. (2020). Overview of the Norwegian Earth System Model (NorESM2) and key climate response of CMIP6 DECK, historical, and scenario simulations. *Geoscientific Model Development*, *13*(12), 6165–6200. https://doi.org/10.5194/gmd-13-6165-2020

Sellar, A. A., Jones, C. G., Mulcahy, J. P., Tang, Y., Yool, A., Wiltshire, A., et al. (2019). UKESM1: Description and evaluation of the U.K. Earth system model. *Journal of Advances in Modeling Earth Systems*, *11*(12), 4513–4558. https://doi.org/10.1029/2019ms001739

Sellers, P. J., Bounoua, L., Collatz, G. J., Randall, D. A., Dazlich, D. A., Los, S. O., et al. (1996). Comparison of radiative and physiological effects of doubled atmospheric CO_2 on climate. *Science*, *271*(5254), 1402–1406. https://doi.org/10.1126/science.271.5254.1402

Shiogama, H., Watanabe, M., Kim, H., & Hirota, N. (2022). Emergent constraints on future precipitation changes. *Nature*, *602*(7898), 612–616. https://doi.org/10.1038/s41586-021-04310-8

Vecchi, G. A., Soden, B. J., Wittenberg, A. T., Held, I. M., Leetmaa, A., & Harrison, M. J. (2006). Weakening of tropical Pacific atmospheric circulation due to anthropogenic forcing. *Nature*, *441*(7089), 73–76. https://doi.org/10.1038/nature04744

Wang, W., Chakraborty, T. C., Xiao, W., & Lee, X. (2021). Ocean surface energy balance allows a constraint on the sensitivity of precipitation to global warming. *Nature Communications*, *12*(1), 2115. https://doi.org/10.1038/s41467-021-22406-7

Wang, W., Lee, X. H., Xiao, W., Liu, S. D., Schultz, N., Wang, Y. W., et al. (2018). Global lake evaporation accelerated by changes in surface energy allocation in a warmer climate. *Nature Geoscience*, *11*(6), 410–414. https://doi.org/10.1038/s41561-018-0114-8

Wentz, F. J., Ricciardulli, L., Hilburn, K., & Mears, C. (2007). How much more rain will global warming bring? *Science*, *317*(5835), 233–235. https://doi.org/10.1126/science.1140746

Woodward, F. I., Lomas, M. R., & Betts, R. A. (1998). Vegetation-climate feedbacks in a greenhouse world. *Philosophical Transactions of the Royal Society B: Biological Sciences*, *353*(1365), 29–39. https://doi.org/10.1098/rstb.1998.0188

Wu, T., Lu, Y., Fang, Y., Xin, X., Li, L., Li, W., et al. (2019). The Beijing climate center climate system model (BCC-CSM): The main progress from CMIP5 to CMIP6. *Geoscientific Model Development*, *12*(4), 1573–1600. https://doi.org/10.5194/gmd-12-1573-2019

Yukimoto, S., Kawai, H., Koshiro, T., Oshima, N., Yoshida, K., Urakawa, S., et al. (2019). The meteorological Research institute Earth system model version 2.0, MRI-ESM2.0: Description and basic evaluation of the physical component. *Journal of the Meteorological Society of Japan Series II*, *97*(5), 931–965. https://doi.org/10.2151/jmsj.2019-051

Zaitchik, B. F., Rodell, M., Biasutti, M., & Seneviratne, S. I. (2023). Wetting and drying trends under climate change. *Nature Water*, *1*(6), 502–513. https://doi.org/10.1038/s44221-023-00073-w

Zhang, X. (2023). In X. Zhang (Ed.), *Dataset for global water cycle-CO_2 feedbacks analysis derived from CMIP6/C4MIP 1pctCO_2 experiments (Version 1.0)* [Dataset]. Figshare. https://doi.org/10.6084/m9.figshare.23894928.v1

Zhang, X., Wang, Y. P., Rayner, P. J., Ciais, P., Huang, K., Luo, Y., et al. (2021). A small climate-amplifying effect of climate-carbon cycle feedback. *Nature Communications*, *12*(1), 2952. https://doi.org/10.1038/s41467-021-22392-w

Zhang, X. J., Tang, Q. H., Zhang, X. Z., & Lettenmaier, D. P. (2014). Runoff sensitivity to global mean temperature change in the CMIP5 Models. *Geophysical Research Letters*, *41*(15), 5492–5498. https://doi.org/10.1002/2014gl060382

Zhang, X. Z., Wang, Y.-P., & Zhang, Y. Q. (2023). Strong nonlinearity of land climate-carbon cycle feedback under a high CO_2 growth scenario. *Earth's Future*, *11*(1). https://doi.org/10.1029/2021ef002499

Zhang, X. Z., Zhang, Y. Q., Ma, N., Kong, D. D., Tian, J., Shao, X. M., & Tang, Q. (2021). Greening-induced increase in evapotranspiration over Eurasia offset by CO_2-induced vegetational stomatal closure. *Environmental Research Letters*, *16*(12), 124008. https://doi.org/10.1088/1748-9326/ac3532

Zhang, X. Z., Zhang, Y. Q., Tian, J., Ma, N., & Wang, Y. P. (2022). CO_2 fertilization is spatially distinct from stomatal conductance reduction in controlling ecosystem water-use efficiency increase. *Environmental Research Letters*, *17*(5), 054048. https://doi.org/10.1088/1748-9326/ac6c9c

Zhang, Y., Li, C., Chiew, F. H. S., Post, D. A., Zhang, X., Ma, N., et al. (2023). Southern Hemisphere dominates recent decline in global water availability. *Science*, *382*(6670), 579–584. https://doi.org/10.1126/science.adh0716

Ziehn, T., Chamberlain, M. A., Law, R. M., Lenton, A., Bodman, R. W., Dix, M., et al. (2020). The Australian Earth system model: ACCESS-ESM1.5. *Journal of Southern Hemisphere Earth Systems Science*, *70*(1), 193–214. https://doi.org/10.1071/ES19035